-RESEARCH PAPER-

International Journal of Mining and Geo-Engineering

IJMGE

IJMGE 57-2 (2023) 149-158

DOI: 10.22059/IJMGE.2022.349301.594998

Reservoir characterization using ensemble-based assimilation methods

Saman Jahanbakhshi [a, *]

[a] *School of Mining Engineering, College of Engineering, University of Tehran, Tehran, Iran.*

Article History:

Received: 29 September 2022.
Revised: 04 November 2022.
Accepted: 13 December 2022.

ABSTRACT

Characterization of large reservoir models with a great number of uncertain parameters is frequently carried out by ensemble-based assimilation methods, due to their computational efficiency, ease of implementation, versatility, and non-necessity of adjoint code. In this study, multiple ensemble-based assimilation techniques are utilized to characterize the well-known PUNQ-S3 model. Accordingly, actual measurements are employed to determine porosity, horizontal and vertical permeabilities, and their associated uncertainties. In consequence, the uncertain parameters of the model will gradually be adapted toward the true values during the assimilation of actual measurements, including bottomhole pressure and production rates of the reservoir. Monotonic reduction of root-mean-squared error and capturing the key points of the maps (such as direction of anisotropy and porosity/permeability contrasts) verify successful estimation of the geostatistical properties of the PUNQ-S3 model during history matching. At the end of the assimilation process, the RMSE values for Deterministic Ensemble Kalman Filter, Ensemble Kalman Filter, Ensemble Kalman Filter with Bootstrap Regularization, Ensemble Transform Kalman Filter Symmetric Solution, Ensemble Transform Kalman Filter Random Rotation, and Singular Evolutive Interpolated Kalman filter are 1.120, 1.153, 1.132, 1.132, 1.129, and 1.113, respectively. In addition to RMSE, the quality of history match as well as prediction of future performance are looked into in order to assess the performance of the assimilation process. Obviously, the results of the ensemble-based assimilation methods closely match the true results both in the history match section and in the future prediction section. Besides, the uncertainty of future predictions is quantified using multiple history-matched realizations. This is due to the fact that Kalman-based filters use a Bayesian framework in the assimilation step. Accordingly, the updated ensemble members are samples of the posterior distribution through which the uncertainty of future performance is assessed.

Keywords: *History matching, Future performance, Uncertainty quantification, Ensemble-based assimilation, PUNQ-S3 model.*

1. Introduction

Conventionally, dynamic reservoir models include several uncertain parameters. Numerous laboratory techniques have been proposed to measure the required unknown parameters. However, these measurements may not be representative at a large scale [1]. Typically, historical measurements are incorporated into the dynamic model in order to characterize reservoir properties under a Bayesian framework which is referred to as history matching [2-4]. Accordingly, history matching is an inverse problem.

Originally, the Kalman filter was developed to estimate unknown variables given the system outputs versus time for linear systems [5]. Subsequently, various variants of the Kalman filter have been proposed for nonlinear systems. Evensen [6] first introduced the ensemble Kalman filter (EnKF), which is the Monte Carlo form of the Kalman filter. Here, a finite number of model realizations are utilized to forecast the covariance matrix as well as approximate the Kalman gain. Consequently, a group of reservoir models is calibrated to match production history in order to accurately assess the uncertainty of future predictions. Ease of implementation, computational efficiency, versatility, and non-necessity of adjoint code make the EnKF well apposite for large models with a great number of uncertain parameters. The First application of EnKF in petroleum engineering was the investigation performed by Lorentzen, et al. [7] wherein uncertain variables of a two-phase flow model in the well, such as liquid hold up and slippage velocity, were estimated so as to match bottom hole pressure response. Afterwards, ensemble-base assimilation methods have been extensively used for the characterization of dynamic reservoir models [2, 8-13].

Nævdal, et al. [14] employed EnKF on a simple two-dimensional reservoir in the North Sea with 14 oil production wells and four gas injectors. The Geostatistical properties of the reservoir model were estimated with acceptable accuracy. To explore the impact of ensemble size, Wen and Chen [15] considered a two-dimensional reservoir with 2,500 grid blocks and utilized EnKF with different ensemble sizes. Moreover, the application of 4D seismic data for reservoir characterization using EnKF was first illustrated by Skjervheim, et al. [16]. Later, Sakov and Oke [17] claimed that the use of perturbed observations in EnKF results in a sub-optimal performance and proposed a simple though highly efficient modification to EnKF, called the Deterministic Ensemble Kalman Filter (DEnKF), wherein the ensemble mean and anomalies are updated separately.

Gao, et al. [18] utilized EnKF and randomized maximum likelihood (RML) for uncertainty quantification in the PUNQ-S3 problem. This investigation disclosed the fact that the proper implementation of RML under a Bayesian framework effectively samples the posterior distribution of the uncertain parameters. Accordingly, both EnKF and RML correctly quantify uncertainty in future predictions, and the true reservoir performance lies within the estimated confidence intervals. Also, the PUNQ-S3 reservoir model has been considered as the test case in many related studies [19-23].

Despite the excessive applications of EnKF in reservoir history

* Corresponding author. *Tel*: (+9821) 82084239, *Fax*: (+9821) 88008838, *E-mail address*:: jahanbakhshi@ut.ac.ir (S. Jahanbakhshi).

matching, some shortcomings are also reported regarding the followings: i) non-Gaussian variables, ii) small ensemble size, and iii) an unsuitable initial ensemble. Accordingly, several remedies have been proposed to overcome these limitations. To handle non-Gaussian variables, it is suggested to parametrize the reservoir properties into another space to reshape the inherent histogram into a Gaussian one [24]. Furthermore, Jahanbakhshi, et al. [10] investigated the effect of initial ensemble members and ensemble size on the posterior distribution of the assimilation methods. Also, iterative EnKF, as a variant of EnKF, has been proposed to minimize the effect of initial ensemble members on the estimated parameters. Akter, et al. [9] investigated the effect of model mismatch on the joint parameter-state estimation. They proposed the addition of an error to the model in the state-space in order to express the discrepancy between the dynamic model and the actual reservoir, as well as introduced forcing data to be used in the noisy systems. Subsequently, the modified EnKF was inspected on a benchmark of tank series model for the assessment purposes. Also, Jo, et al. [2] combined the machine learning algorithms with EnKF and proposed an assisted history matching workflow well-suited for large scale reservoir models, as well as non-Gaussian variables. Subsequently, the suggested workflow was examined on a deep-water lobe system. In a different study, Delijani, et al. [25] presented an adaptive thresholding procedure for covariance localization of EnKF. In this way, a smaller ensemble size could be implemented without the problem of spurious correlation in the forecast covariance matrix. Similarly, Watanabe and Datta-Gupta [21] demonstrated that the successful implementation of covariance localization drastically depends on the dynamics of multi-phase fluid flow, as well as the type of the measurement data. Consequently, they proposed covariance localization based on the phase streamlines.

In this study, different ensemble-based assimilation techniques are utilized to characterize the PUNQ-S3 model. Accordingly, historical measurements are employed so as to estimate porosity, horizontal, and vertical permeabilities in a sequential manner. As a result, uncertain parameters of the mathematical model will be gradually adapted toward the true values during assimilation of actual measurements, including bottomhole pressure and production rates of the reservoir. The Monotonic reduction of root-mean-squared error and capturing the key points on the maps (such as direction of anisotropy and porosity/permeability contrasts) verify the successful estimation of the geostatistical properties of the PUNQ-S3 model during history matching. In addition to RMSE, the quality of history match, as well as the prediction of future performance are looked into so as to assess the performance of the assimilation process. Obviously, the results of the ensemble-based assimilation methods closely match the true results both in the history match section and in the future prediction section. Besides, the uncertainty of future predictions is quantified. This is due to the fact that Kalman-based filters use a Bayesian framework in the assimilation step. Accordingly, updated ensemble members are samples of the posterior distribution through which the uncertainty of the future performance is assessed.

This article is organized as follows: ensemble-based assimilation methods are described in Section 2. Section 3 elaborates on the PUNQ-S3 reservoir model with its production data and initial realizations. Next, the results of the model calibration as well as the prediction of future performance are discussed in Section 4. Afterwards, Section 5 summarizes the conclusions.

2. Methodology

2.1. System state-space

State-space of the system is represented as [5, 10]:

$$x_k = M_k(x_{k-1}, u_k) \tag{1}$$

$$d_k = H_k x_k + D_k \tag{2}$$

M_k is the mathematical model of the reservoir, $x_k = \left[m^T, s^T, \tilde{d}^T\right]_k^T$ represents the state vector where m is model parameters, s shows system states, and $\tilde{d}$ represents predicted observations. Also, u_k is the boundary conditions, and d_k stands for real observations. $H_k \equiv [O \quad I]_k$ relates the real observations to the state vector. Furthermore, $D_k = \left[\varepsilon_1, \varepsilon_2, \dots, \varepsilon_{n_d}\right]_k$ shows the perturbations vector obtained using a zero-mean Gaussian distribution with a covariance matrix R_k; $D_k \sim N(0, R_k)$.

In Section 3, the reservoir model along with boundary conditions is elaborated.

2.2. Ensemble Kalman filter (EnKF)

Details of EnKF method is provided by Evensen [26]. The forecast ensemble is calculated as:

$$A^f = \left[x_1^f - x^f, x_2^f - x^f, \dots, x_N^f - x^f\right] \tag{3}$$

$$x^f = \frac{1}{N}\sum_{i=1}^{N} x_i^f \tag{4}$$

The covariance matrix of the forecast error is:

$$P^f = \frac{1}{N-1}\sum_{i=1}^{N}\left(x_i^f - x^f\right)\left(x_i^f - x^f\right)^T = \frac{1}{N-1}A^f\left(A^f\right)^T \tag{5}$$

Then, equation of Kalman filter becomes:

$$x^a = x^f + K\left(d - Hx^f\right) \tag{6}$$

$$A_i^a = A_i^f + K\left(D^{(i)} - HA_i^f\right); \quad i = 1,2,\dots,N \tag{7}$$

$$X_i^a = x^a + A_i^a; \quad i = 1,2,\dots,N \tag{8}$$

where $K$is the Kalman gain matrix. Thus, covariance matrix of the analysis error becomes:

$$P^a = \frac{1}{N-1}\sum_{i=1}^{N}(x_i^a - x^a)(x_i^a - x^a)^T = \frac{1}{N-1}A^a(A^a)^T \tag{9}$$

Minimization of P^aresults in:

$$K = P^f H^T\left(HP^f H^T + R\right)^{-1} \tag{10}$$

$$P^a = (I - KH)P^f \tag{11}$$

2.3. Deterministic ensemble Kalman filter (DEnKF)

Sakov and Oke [17] presented DEnKF wherein the ensemble mean is updated similar to EnKF while updated anomalies are obtained from:

$$A^a = A^f - \frac{1}{2}KHA^f \tag{12}$$

2.4. Ensemble transform Kalman filter (ETKF)

Here, updated anomalies are calculated by a transformation matrix $\boldsymbol{T}$:

$$A^a = A^f T \tag{13}$$

A generic form of the transformation matrix is [27]:

$$T = T^s U \tag{14}$$

$$T^s = \left[I + \frac{1}{N-1}\left(HA^f\right)^T R^{-1} HA^f\right]^{-\frac{1}{2}} \tag{15}$$

U is an orthonormal mean-preserving matrix in which

$$UU^T = I \tag{16}$$

$$U1 = 1 \tag{17}$$

If $U = I$, the method is called the symmetric solution (ETKF-SS). Otherwise, it is labeled as the random rotation (ETKF-RR) [28].

2.5. EnKF with bootstrap regularization (EnKF-BR)

In this method, the forecast ensemble is regarded as the population, and a number of N_B samples are generated by bootstrapping so as to compute the confidence level for each component of the Kalman gain matrix (K_m). Therefore, K_m is calculated for each ensemble, and its variance is also computed:

$$\sigma_{K_{i,j}}^2 = \frac{\sum_{m=1}^{N_B}\left(K_{i,j,m} - \overline{K}_{i,j}\right)^2}{N_B} \tag{18}$$

Thus, the squared coefficient of variation for each element of K_m and the associated confidence factor become:

$$C_{v_{i,j}}^2 = \frac{\sigma_{K_{i,j}}^2}{\overline{K}_{i,j}^2} \quad (19)$$

$$\alpha_{K_{i,j}}^2 = \frac{1}{1+\left(1+\frac{1}{\sigma_\alpha^2}\right)C_{v_{i,j}}^2} \quad (20)$$

A value of $\sigma_\alpha^2 = 0.36$ gives the best results, as discussed by Zhang and Oliver [29]. Finally, the screened Kalman gain (K^{SK}) is utilized to calculate the updated ensemble,

$$\mathrm{K}^{SK} = \alpha_{\mathrm{K}} \circ \overline{\mathrm{K}} \quad (21)$$

2.6. Singular evolutive interpolated Kalman (SEIK) filter

Here, the covariance matrix of the forecast error is decomposed to [30]:

$$P^f = LGL^T \quad (22)$$

$$L = X^f \tilde{T} \quad (23)$$

$$G = \left(N\tilde{T}^T\tilde{T}\right)^{-1} \quad (24)$$

wherein $X^f = \left[x_1^f, x_2^f, \dots, x_N^f\right]$ shows the forecast ensemble matrix and matrix $\tilde{T}$ is:

$$\tilde{T} = \begin{bmatrix} I_{(N-1)\times(N-1)} \\ O_{1\times(N-1)} \end{bmatrix} - \frac{1}{N}\left[1_{N\times(N-1)}\right] \quad (25)$$

Accordingly, the Kalman gain is obtained:

$$K = LW(HL)^T R^{-1} \quad (26)$$

$$W^{-1} = G^{-1} + (HL)^T R^{-1} HL \quad (27)$$

The Kalman gain is utilized to calculate the updated ensemble mean by the use of Eq. 6. Afterwards, updated anomalies are computed from [31]:

$$A^a = \sqrt{N} L C^{-1} \Omega^T \quad (28)$$

$$(C^{-1})^T C^{-1} = W^{-1} \quad (29)$$

where Ω is a matrix which is orthogonal and orthonormal to the vector $1_{N\times1}$.

3. Description of the PUNQ-S3 reservoir model

The PUNQ-S3 model is a three-dimensional model established from an industrial survey on an actual field in the North Sea as a part of the PUNQ project (Production forecasting with Uncertainty Quantification). The goal of the PUNQ project was to assess different methods of uncertainty quantification in the history matching process. Accordingly, the PUNQ-S3 model has been intensively utilized as a benchmark in distinct inverse techniques in the petroleum literature. Details of the PUNQ-S3 model are provided by Floris, et al. [32].

The model is an anticline where the middle oil layer is surrounded by gas at the top and water at the bottom. Corner-point geometry is utilized to represent the structure of the field. The model consists of 19 × 28 × 5 grid blocks of size 180 × 180 m2 with 1761 active blocks. The East and south of the PUNQ-S3 model are restricted by faults and a strong aquifer bounds the model on the north and the west, suppressing the need of for injection wells. Fig. 1 illustrates the top view of the field together with the locations of six producers (PRO-5, PRO-12, PRO-4, PRO-1, PRO-11, PRO-15) in the vicinity of the gas-oil contact. Production wells are completed through the fourth and fifth layers.

In the PUNQ project, production data of the first eight years together with geological descriptions and hard data at well locations were available to the partners so as to calibrate the reservoir model. The updated model is then used to forecast the future performance of the field and predict cumulative oil production after 16.5 years.

3.1. Production data

The Production schedule of each well consists of four steps [32, 33]:

1. Initially, an extended well test is conducted with four production intervals, each one lasting for three months.

2. Subsequently, a period of three-year shut-in is conducted.

3. Afterwards, a period of four-year production is conducted wherein the target rate of oil production is 150 sm^3/day with minimum bottom hole pressure of 120 bar as the secondary constraint. Also, whenever production gas-oil ratio exceeds 200 sm^3/sm^3, target rate of oil production will be decreased by 25%.

4. Finally, a period of two-week shut-in is conducted at the end of each year with the aim of measuring reservoir static pressure.

The Measurement data, depicted in Fig. 2, include well oil production rate (WOPR), well water cut (WWCT), well gas-oil ratio (WGOR), and well bottom hole pressure (WBHP). It is assumed that measurement error is a white Gaussian noise with mean zero. Also, the standard deviation (STD) of the noise is reported in Table 1. There are 20 asynchronous assimilation cycles throughout the eight-year production history where the corresponding times and data are represented in Table 2.

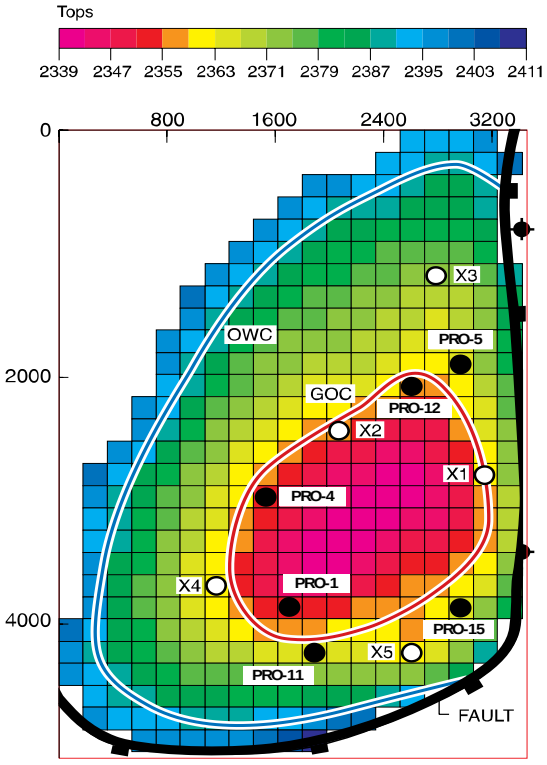

Fig. 1 - Top structure map of the PUNQ-S3 model [32].

Accordingly, the state vector for the PUNQ-S3 model becomes:

$$x = \left[m^T, s^T, \tilde{d}^T\right]^T \quad (30)$$

where,

$$m = [\phi^T, ln\, k_h^T, ln\, k_v^T]^T \quad (31)$$

$$s = \left[P_o^T, S_w^T, S_g^T, R_s^T\right]^T \quad (32)$$

$$\tilde{d} = [\mathrm{WBHP}^T, \mathrm{WGOR}^T, \mathrm{WWCT}^T, \mathrm{WOPR}^T]^T \quad (33)$$

Here, ϕ shows porosity, as well as k_h and k_v are horizontal and vertical permeabilities. As the distribution of permeability is frequently log-normal, $ln\, k$ is considered in the state vector so as to ensure

Gaussian distribution of the variables. Also, P_o is oil pressure, S_w shows water saturation, S_g shows gas saturation, and R_s represents solution gas-oil ratio in each grid block.

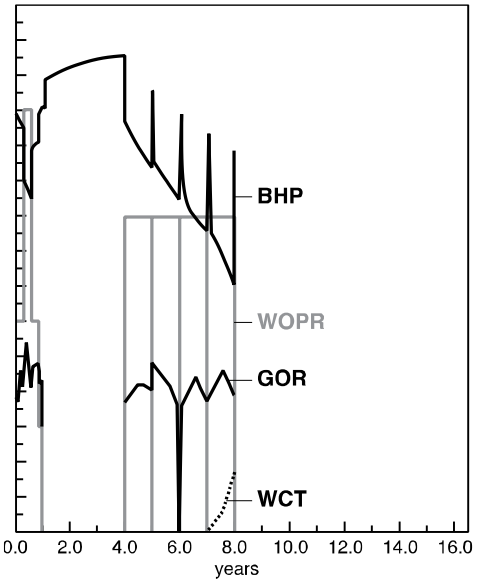

Fig. 2 - Production history of the PUNQ-S3 model [32].

Table 1. Standard deviation of the white Gaussian noise.

Measurement	STD
WOPR (sm^3/day)	1.0×10^{-4}
Shut-in WBHP (bar)	1.0
Flowing WBHP (bar)	3.0
WWCT (-)	0.01
WGOR (-) (before gas breakthrough)	10%
WGOR (-) (after gas breakthrough)	25%

3.2. Initial realizations

To generate initial realizations of porosity, values of normalized porosity at the well locations are obtained from the reference PUNQ-S3 model, represented in Table 3. Afterwards, sequential Gaussian simulation (*sgsim*) with a spherical anisotropic variogram is utilized to produce initial realizations of normalized porosity using the SGeMS software [34, 35]. Finally, actual values of porosity are calculated:

$$\phi = \phi_N \times \sigma_\phi + \mu_\phi \tag{34}$$

where ϕ_N shows normalized porosity, ϕ is the actual porosity, μ_ϕ and σ_ϕ are mean and standard deviation of the porosity map reported in Table 4; respectively. Based on the porosity and permeability values at the well locations, horizontal and vertical permeabilities are calculated from porosity with the following relations [36]:

$$log_{10}(k_h) = 9.02\phi + 0.77 \tag{35}$$

$$k_v = 0.31k_h + 3.12 \tag{36}$$

4. Results and discussions

Here, DEnKF, EnKF, EnKF-BR, ETKF-RR, ETKF-SS, and SEIK filters are utilized to estimate porosity and permeabilities of the grid blocks, as well as to predict future performance of the PUNQ-S3 model. An ensemble size of $N = 100$ is considered for the assimilation process, and the true model is considered as the reference case.

4.1. Porosity and permeability estimation

To evaluate the performance of the ensemble-based assimilation methods, root-mean-squared error (RMSE) and ensemble spread are computed at each cycle.

$$\text{RMSE} = \sqrt{\frac{1}{N_{grid}}\sum_{i=1}^{N_{grid}}\frac{1}{N}\sum_{j=1}^{N}\left(m_{i,j} - m_i^{true}\right)^2} \tag{37}$$

$$\text{spread} = \sqrt{\frac{1}{N_{grid}}\sum_{i=1}^{N_{grid}}\frac{1}{N}\sum_{j=1}^{N}\left(m_{i,j} - \bar{m}_i\right)^2} \tag{38}$$

where N_{grid} is the number of grid blocks, m is the updated parameter field at each assimilation cycle, m^{true} shows the reference field and $\bar{m}$ is the mean of the updated fields. RMSE and spread are calculated separately for porosity, $ln\, k_h$, and $ln\, k_v$, and their average values are represented at each assimilation cycle in Fig. 3. Clearly, RMSE decreases monotonically versus time which verifies that the realizations get closer to the reference case as the assimilation proceeds and more measurements are incorporated into the prior model. Consequently, if more historical measurement were available, RMSE would decrease further and more accurate estimation of uncertain model parameters would be obtained. This is in agreement with the Bayesian framework in which the prior model will be updated to the posterior one whenever new dynamical measurement becomes available. At the end of the assimilation process, the RMSE values for DEnKF, EnKF, EnKF-BR, ETKF-RR, ETKF-SS, and SEIK filters are 1.120, 1.153, 1.132, 1.132, 1.129, and 1.113, respectively. Moreover, the spread of the realizations reduces continuously which indicates that the uncertainty of the updated model further decreases. Obviously, the SEIK filter has the lowest RMSE and EnKF-BR preserves the highest spread.

Table 2. Production data used in the assimilation process.

Step	Time (days)	WBHP	WGOR	WWCT	WOPR
1	1.01	6	-	-	6
2	91	6	-	-	6
3	182	6	-	-	6
4	274	6	-	-	6
5	366	6 (shut-in)	-	-	6
6	1461	6 (shut-in)	-	-	6
7	1642	-	6	-	6
8	1826	6	6	-	6
9	1840	6 (shut-in)	-	-	6
10	1841	-	6	-	6
11	2008	-	6	-	6
12	2192	6	6	-	6
13	2206	6 (shut-in)	-	-	6
14	2373	-	6	-	6
15	2557	6	6	-	6
16	2571	6 (shut-in)	-	-	6
17	2572	-	-	1	6
18	2738	-	6	-	6
19	2922	6	6	6	6
20	2936	6 (shut-in)	-	-	6

Table 3. Normalized porosity values at the well locations.

Well	Layer 1	Layer 2	Layer 3	Layer 4	Layer 5
PRO-1	-0.5	-0.4	-0.4	1.0	1.0
PRO-4	0.8	-0.5	-0.2	1.3	0.6
PRO-5	1.0	-0.3	0.7	0.9	-0.4
PRO-11	-0.4	0.2	0.9	0.6	0.1
PRO-12	-0.6	0.8	-0.3	1.4	0.9
PRO-15	1.2	0.6	0.4	2.0	1.2

Table 4. Mean and standard deviation values of the porosity map [19].

Parameter	Layer 1	Layer 2	Layer 3	Layer 4	Layer 5
Mean	0.15	0.08	0.15	0.11	0.17
STD	0.08	0.04	0.08	0.05	0.08

The PUNQ-S3 model has five layers and within each layer porosity, horizontal, and vertical permeabilities are estimated. Therefore, a number of 15 maps are required so as to illustrate the results of the assimilation process. However, only the estimated maps of the first layer are depicted here. Fig. 4 compares the estimated porosity map of layer 1 (average of all the updated realizations) with the true one. Clearly, the final estimated maps are in close agreement with the true map, and key points of the map (such as the direction of anisotropy and porosity contrasts) are well captured. Specifically, DEnKF, EnKF-BR, and SEIK filters have outperformed and better cope with the porosity contrasts of the true map. Similarly, Fig. 5 and Fig. 6 represent maps of $ln\, k_h$ and $ln\, k_v$, respectively. Again, DEnKF and SEIK filters surpass the other filters and well capture the permeability contrasts. Furthermore, the estimated porosity and permeabilities at the grid blocks around the production wells correspond exactly the true ones. This is due to the fact that properties of the surrounding blocks have the highest impact on the production data. In other words, the information content of the measurements reduces as the distance from observation location increases. This is the main idea for those researches in the realm of the covariance localization [21, 37-39]. Moreover, the average of the initial realizations is highly smooth as a consequence of the random generation of the initial ensemble by the use of *sgsim* algorithm.

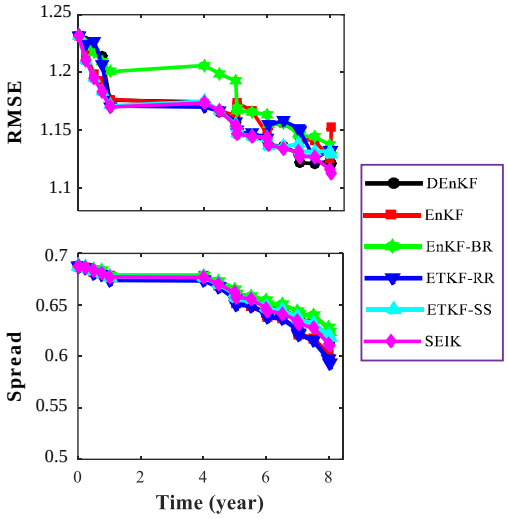

Fig. 3 - RMSE and spread versus assimilation cycle.

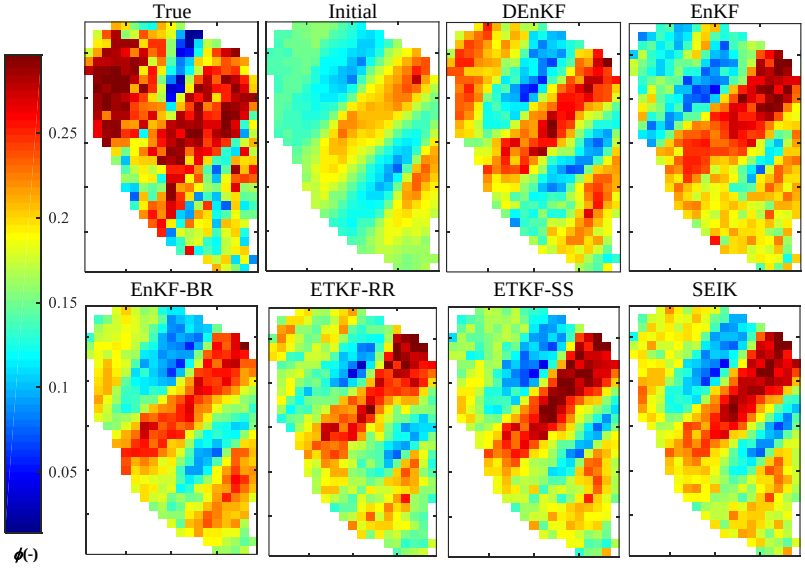

Fig. 4 -The Estimated porosity map of layer 1 of the PUNQ-S3 model.

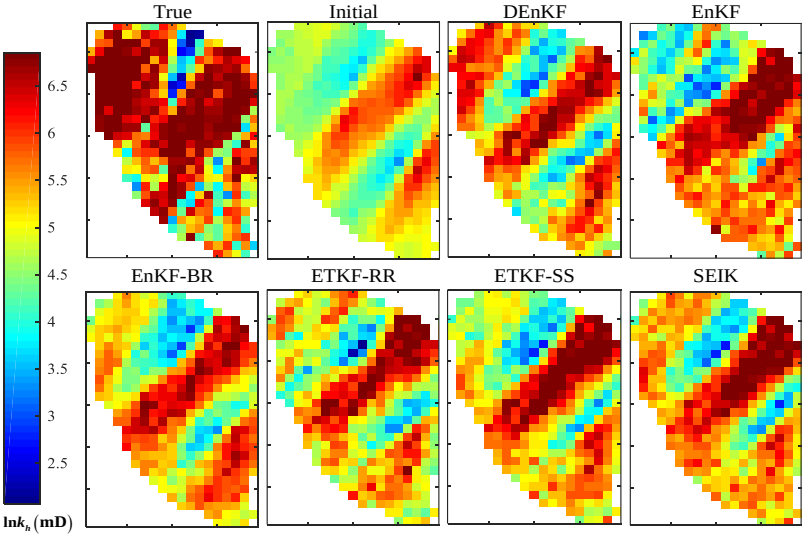

Fig. 5 - The Estimated ln k_h map of layer 1 of the PUNQ-S3 model.

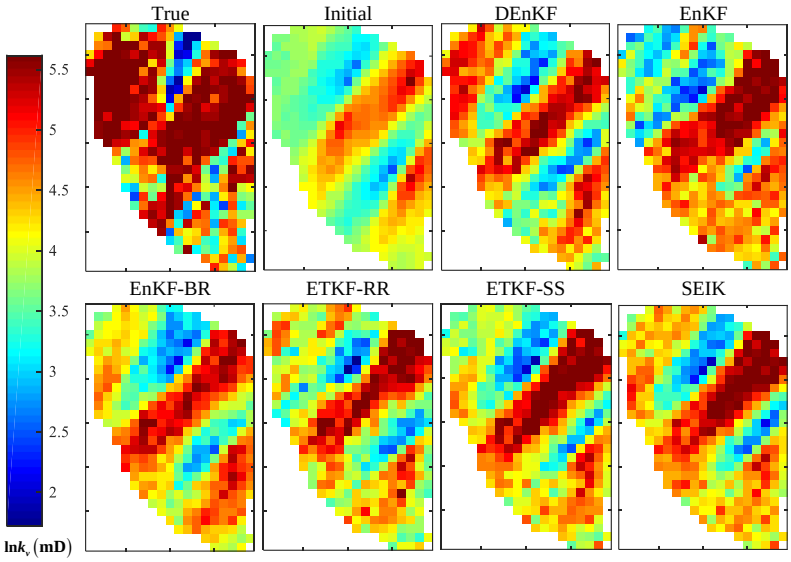

Fig. 6 - The Estimated ln k_v map of layer 1 of the PUNQ-S3 model.

4.2. Future performance prediction

In addition to RMSE and spread, the quality of history match along with prediction of the future performance are two main criteria for the assessment of filter performance. Due to the numerous numbers of available figures, only the production data of well PRO-11, as well as the field cumulative oil and water productions are illustrated here.

Figs. 7-10 represent the bottom hole pressure, gas-oil ratio, water cut, and oil production rate of well PRO-11, respectively. Here, the results of the initial ensemble are illustrated with gray curves. The black curves represent the results of the updated ensemble. Due to the non-linearity of the mathematical model, each of the updated realizations is separately employed in the reservoir simulator so as to predict future performance of the field. Also, the red lines express actual measurements from the true model (wherein true values of porosity and permeability are employed). Moreover, the cyan and the blue lines respectively stand for the average results obtained by the initial and updated ensembles. A vertical line separates the time period into two sections: data used for model calibration (left) and data used for the evaluation of future performance prediction.

Expectedly, the results of the initial ensemble have the highest spread. Also, the use of the initial ensemble overestimates WGOR and WWCT (Fig. 8 and Fig. 9) and underestimates WBHP and WOPR (Fig. 7 and Fig. 10). In Fig. 7, all the ensemble-based assimilation methods overestimate WBHP, and the SEIK filter is the closest to the true results. Furthermore, the ensemble spread to the left of the vertical line (model calibration section) is much smaller than that to the right of the vertical line (future performance prediction section). This is due to the fact that the model calibration by the use of actual measurements has reduced the uncertainty of the model. Also, the uncertainty of the future performance can be quantified by the use of the ensemble spread. In Fig. 8, DEnKF, EnKF, EnKF-BR, and ETKF-RR underestimate the true results, while the ETKF-SS and SEIK filters overestimate them. Again, the results of EnKF and SEIK filters are more accurate.

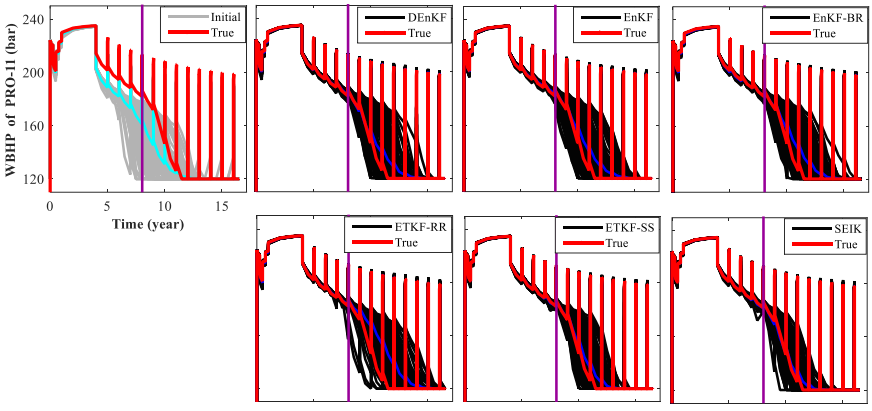

Fig. 7 - The History match and prediction of the future performance for the WBHP of PRO-11.

In Fig. 9, all of the assimilation methods underestimate the water cut in well PRO-11 and ETKF-RR has the largest discrepancy. It is worth mentioning that the observation data has no information about water breakthrough in well PRO-11. However, DEnKF, EnKF, EnKF-BR, ETKF-SS, and SEIK filters have successfully predicted the water cut in this well. This further confirms the successful calibration of the field model by the use of the measured dynamic data.

In Fig. 10, all of the assimilation methods overestimate the oil production rate in well PRO-11, and ETKF-SS and SEIK filters are the closest to the true results. Also, in the model calibration section, all the updated realizations show a constant production rate of 150 sm^3/day.

Fig. 11 and Fig. 12 represent the cumulative field oil and water

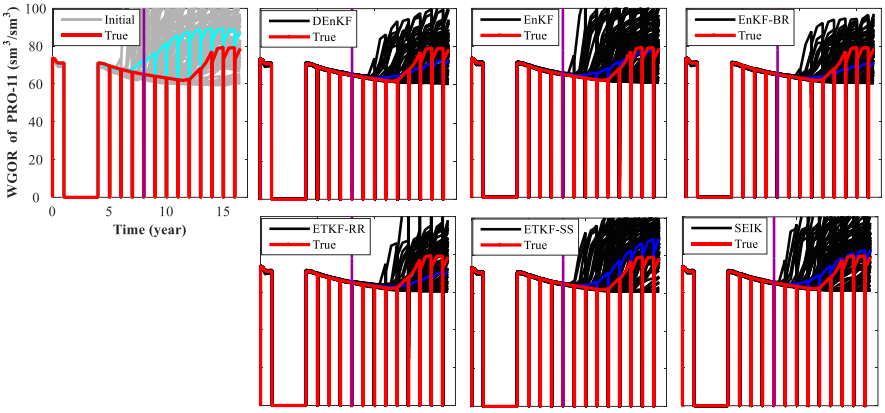

Fig. 8 - The History match and prediction of the future performance for the WGOR of PRO-11.

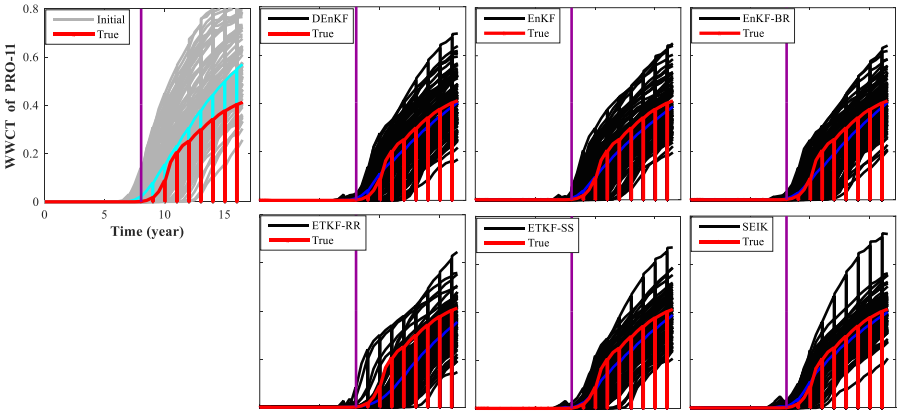

Fig. 9 -The History match and prediction of the future performance for the WWCT of PRO-11.

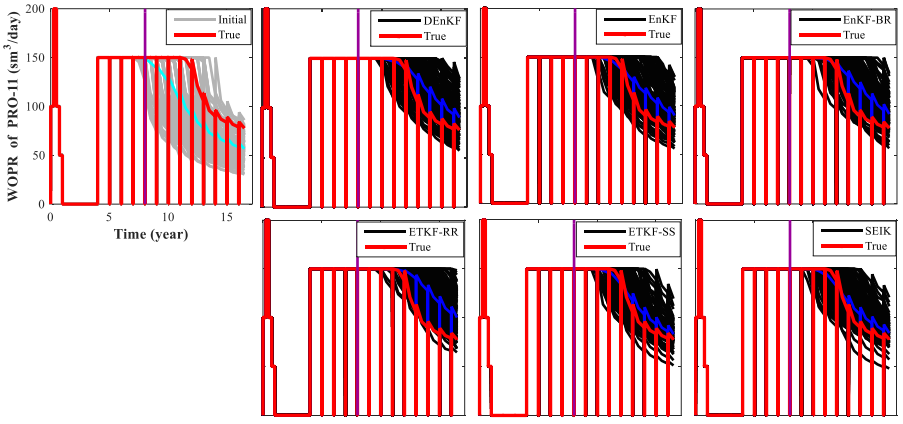

Fig. 10 - The History match and prediction of the future performance for the WOPR of PRO-11.

productions, respectively. The Results of the initial ensemble underestimate both FOPT and FWPT. In Fig. 11, the uncertainty of the updated model has reduced significantly and there is a close agreement between the updated realizations and the true results. In Fig. 12, the DEnKF has overestimated the true FWPT, while the other ones have underestimated it. Here, ETKF-RR has the highest accuracy compared to the true model.

As discussed previously in the description of the PUNQ project, data from the first eight years were available to calibrate the reservoir model. Accordingly, the updated model is then used to forecast the future performance of the field after 16.5 years. Table 5 represents the mean and standard deviation values of the cumulative field oil, gas, and water productions after 16.5 years. Obviously, ensemble-based assimilation methods have successfully predicted the future performance quantified the associated uncertainty. This is due to the fact that the assimilation step in the Kalman filter uses a Bayesian framework [10]. Therefore, the updated ensemble members are samples of the posterior distribution through which the uncertainty of the future performance is assessed [40].

Based on the above-mentioned discussions, all the ensemble-based Kalman filters exhibit promising results, which make them suitable for the characterization of large reservoir models. Specifically, the SEIK filter has outperformed the other ones in the characterization of the PUNQ-S3 reservoir model in this study. Accordingly, the SEIK filter has

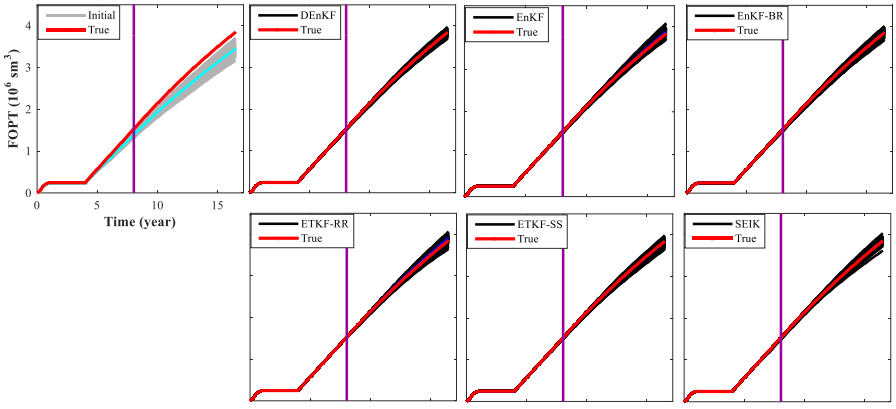

Fig. 11 - The History match and prediction of the future performance for the cumulative field oil production.

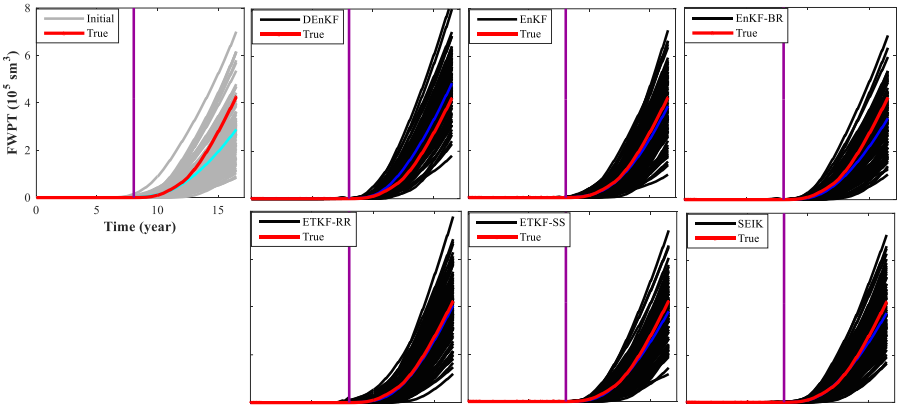

Fig. 12 - The History match and prediction of the future performance for the cumulative field water production.

Table 5. The Mean and standard deviation values of FOPT, FGPT and FWPT after 16.5 years (10^6 sm^3).

	True		Initial	DEnKF	EnKF	EnKF-BR	ETKF-RR	ETKF-SS	SEIK
FOPT	3.85	Mean	3.45	3.84	3.89	3.86	3.91	3.84	3.85
		STD	0.12	0.06	0.07	0.08	0.08	0.07	0.07
FGPT	0.35	Mean	0.29	0.33	0.35	0.34	0.34	0.34	0.34
		STD	0.01	0.01	0.01	0.01	0.01	0.01	0.01
FWPT	0.43	Mean	0.29	0.49	0.39	0.34	0.41	0.38	0.38
		STD	0.16	0.12	0.14	0.12	0.13	0.11	0.12

resulted in a more accurate estimation of porosity and permeability maps, and it is the closest to the true model in the history match section, and also accurately predicts the future performance. Therefore, the SEIK filter is highly recommended for the characterization of complex reservoir models by the use of measured dynamic data.

5. Conclusion

In this study, six different ensemble-based assimilation techniques were utilized to characterize the PUNQ-S3 model. Historical measurements, including bottomhole pressure and production rates, were employed to estimate porosity, horizontal, and vertical permeabilities. Consequently, the uncertain parameters of the model were gradually adjusted toward the true values during the assimilation of historical data. Obviously, the key points of the maps (such as the direction of anisotropy and porosity/permeability contrasts) were captured accurately, and RMSE between the estimated and the true maps decreased monotonically, which verified the successful estimation of porosity and permeabilities in the PUNQ-S3 model during history matching.

In addition to RMSE, the quality of history match as well as the prediction of the future performance were inspected so as to assess the performance of the assimilation process. Clearly, the results of the ensemble-based assimilation methods closely matched the true results both in the history match section as well as in the future prediction section.

There are a considerable number of distinct benefits regarding the ensemble-based Kalman filters. To start with, ease of implementation, computational efficiency, versatility, and non-necessity of adjoint code make the ensemble-based Kalman filters well apposite for large models with a great number of uncertain parameters. Next, these methods are recursive and sequential, meaning that only the latest measurement is assimilated with the current prior model. To follow, ensemble-based assimilation methods use the simulation model as a black-box to

perform the time update in the forecast step. Consequently, they are compatible with any complex reservoir models and various reservoir simulators. Finally, the uncertainty of the future predictions is also quantified by the use of multiple history-matched realizations. This is owing to the fact that Kalman-based filters use a Bayesian framework in the assimilation step. Therefore, updated ensemble members are samples of the posterior distribution through which the uncertainty of the future performance is assessed.

REFERENCES

[1] Tokhmechi B, J Nasiri, H Azizi, M Rabiei, V Rasouli. Wavelet Neural Network: A Hybrid Method in Modeling Heterogeneous Reservoirs. Int J Min Geo-Eng. 53 (2019) 203-11, doi: http://dx.doi.org/10.22059/ijmge.2018.259499.594745.

[2] Jo H, W Pan, JE Santos, H Jung, MJ Pyrcz. Machine learning assisted history matching for a deepwater lobe system. J Petrol Sci Eng. 207 (2021) 109086, doi: https://doi.org/10.1016/j.petrol.2021.109086.

[3] Li Y, M Onur. INSIM-BHP: A physics-based data-driven reservoir model for history matching and forecasting with bottomhole pressure and production rate data under waterflooding. J Comput Phys. 473 (2022) 111714, doi: https://doi.org/10.1016/j.jcp.2022.111714.

[4] Ma X, K Zhang, J Wang, C Yao, Y Yang, H Sun, et al. An Efficient Spatial-Temporal Convolution Recurrent Neural Network Surrogate Model for History Matching. SPE J. 27 (2022) 1160-75, doi: https://doi.org/10.2118/208604-PA.

[5] Lewis JM, S Lakshmivarahan, S Dhall. Dynamic data assimilation: a least squares approach. 1st ed. Cambridge University Press, New York, 2006.

[6] Evensen G. Sequential data assimilation with a nonlinear quasi-geostrophic model using Monte Carlo methods to forecast error statistics. J Geophys Res-Oceans. 99 (1994) 10143-62, doi: http://dx.doi.org/10.1029/94JC00572.

[7] Lorentzen R, K Fjelde, F Jonny, A Lage, N Geir, E Vefring. Underbalanced and low-head drilling operations: Real time interpretation of measured data and operational support. In: SPE Annual Technical Conference and Exhibition. New Orleans, Louisiana (2001), doi: https://doi.org/10.2118/71384-MS.

[8] Chang H, D Zhang, Z Lu. History matching of facies distribution with the EnKF and level set parameterization. J Comput Phys. 229 (2010) 8011-30, doi: http://dx.doi.org/10.1016/j.jcp.2010.07.005.

[9] Akter F, S Imtiaz, S Zendehboudi, K Hossain. Modified Ensemble Kalman filter for reservoir parameter and state estimation in the presence of model uncertainty. J Petrol Sci Eng. 199 (2021) 108323, doi: https://doi.org/10.1016/j.petrol.2020.108323.

[10] Jahanbakhshi S, MR Pishvaie, RB Boozarjomehry. Impact of initial ensembles on posterior distribution of ensemble-based assimilation methods. J Petrol Sci Eng. 171 (2018) 82-98, doi: https://doi.org/10.1016/j.petrol.2018.07.022.

[11] Abdolhosseini H, E Khamehchi. History matching using traditional and finite size ensemble Kalman filter. J Nat Gas Sci Eng. 27 (2015) 1748-57, doi: http://dx.doi.org/10.1016/j.jngse.2015.10.041.

[12] Zhang Y, Z Fan, D Yang, H Li, S Patil. Simultaneous estimation of relative permeability and capillary pressure for PUNQ-S3 model with a damped iterative-ensemble-Kalman-filter technique. SPE J. 22 (2017) 971 - 84, doi: https://doi.org/10.2118/177846-PA.

[13] Xue L, S Gu, L Mi, L Zhao, Y Liu, Q Liao. An automated data-driven pressure transient analysis of water-drive gas reservoir through the coupled machine learning and ensemble Kalman filter method. J Petrol Sci Eng. 208 (2022) 109492, doi: https://doi.org/10.1016/j.petrol.2021.109492.

[14] Nævdal G, T Mannseth, EH Vefring. Near-well reservoir monitoring through ensemble Kalman filter. In: SPE/DOE Improved Oil Recovery Symposium. Tulsa, Oklahoma (2002), doi: https://doi.org/10.2118/75235-MS.

[15] Wen X-H, W Chen. Real-time reservoir model updating using ensemble Kalman filter. SPE J. 11 (2006) 431-42, doi: http://dx.doi.org/10.2118/92991-PA.

[16] Skjervheim JA, G Evensen, SI Aanonsen, BO Ruud, TA Johansen. Incorporating 4D seismic data in reservoir simulation models using ensemble Kalman filter. SPE J. 12 (2007) 282-92, doi: https://doi.org/10.2118/95789-PA.

[17] Sakov P, PR Oke. A deterministic formulation of the ensemble Kalman filter: an alternative to ensemble square root filters. Tellus. 60 (2008) 361-71, doi: http://dx.doi.org/10.1111/j.1600-0870.2007.00299.x.

[18] Gao G, M Zafari, AC Reynolds. Quantifying uncertainty for the PUNQ-S3 problem in a Bayesian setting with RML and EnKF. SPE J. 11 (2006) 506-15, doi: http://dx.doi.org/10.2118/93324-PA.

[19] Gu Y, DS Oliver. History matching of the PUNQ-S3 reservoir model using the ensemble Kalman filter. SPE J. 10 (2005) 217 - 24, doi: https://doi.org/10.2118/89942-PA.

[20] Lee K, S Jung, T Lee, J Choe. Use of clustered covariance and selective measurement data in ensemble smoother for three-dimensional reservoir characterization. J Energy Resour Technol. 139 (2017), doi: https://doi.org/10.1115/1.4034443.

[21] Watanabe S, A Datta-Gupta. Use of phase streamlines for covariance localization in ensemble Kalman filter for three-phase history matching. SPE Reserv Eval Eng. 15 (2012) 273-89, doi: https://doi.org/10.2118/144579-MS.

[22] Arouri Y, M Sayyafzadeh. An adaptive moment estimation framework for well placement optimization. Computat Geosci. 26 (2022) 957–73, doi: https://doi.org/10.1007/s10596-022-10135-9.

[23] Raji S, A Dehnamaki, B Somee, MR Mahdiani. A new approach in well placement optimization using metaheuristic algorithms. J Petrol Sci Eng. 215 (2022) 110640, doi: https://doi.org/10.1016/j.petrol.2022.110640.

[24] Lorentzen RJ, G Nævdal, A Shafieirad. Estimating facies fields by use of the ensemble Kalman filter and distance functions--applied to shallow-marine environments. SPE J. 3 (2013) 146-58, doi: http://dx.doi.org/10.2118/143031-PA.

[25] Delijani EB, MR Pishvaie, RB Boozarjomehry. Subsurface characterization with localized ensemble Kalman filter employing adaptive thresholding. Adv Water Resour. 69 (2014) 181-96, doi: http://dx.doi.org/10.1016/j.advwatres.2014.04.011.

[26] Evensen G. Data assimilation: the ensemble Kalman filter. 2nd ed. Springer Science & Business Media, New York, 2009.

[27] Bishop CH, BJ Etherton, SJ Majumdar. Adaptive sampling with the ensemble transform Kalman filter. Part I: Theoretical aspects. Mon Weather Rev. 129 (2001) 420-36, doi: http://dx.doi.org/10.1175/1520-0493(2001)129<0420:ASWTET>2.0.CO;2.

[28] Sakov P, PR Oke. Implications of the form of the ensemble transformation in the ensemble square root filters. Mon Weather Rev. 136 (2008) 1042-53, doi: http://dx.doi.org/10.1175/

2007MWR2021.1.

[29] Zhang Y, DS Oliver. Improving the ensemble estimate of the Kalman gain by bootstrap sampling. Math Geosci. 42 (2010) 327-45, doi: http://dx.doi.org/10.1007/s11004-010-9267-8.

[30] Nerger L, T Janji, J Schröter, W Hiller. A unification of ensemble square root Kalman filters. Mon Weather Rev. 140 (2012) 2335-45, doi: http://dx.doi.org/10.1175/MWR-D-11-00102.1.

[31] Sun AY, A Morris, S Mohanty. Comparison of deterministic ensemble Kalman filters for assimilating hydrogeological data. Adv Water Resour. 32 (2009) 280-92, doi: http://dx.doi.org/10.1016/j.advwatres.2008.11.006.

[32] Floris FJT, MD Bush, M Cuypers, F Roggero, AR Syversveen. Methods for quantifying the uncertainty of production forecasts: a comparative study. Pet Geosci. 7 (2001) 87-96, doi: http://dx.doi.org/10.1144/petgeo.7.S.S87.

[33] Verga F, M Cancelliere, D Viberti. Improved application of assisted history matching techniques. J Petrol Sci Eng. 109 (2013) 327-47, doi: http://dx.doi.org/10.1016/j.petrol.2013.04.021.

[34] Remy N, A Boucher, J Wu. Applied geostatistics with SGeMS: A user's guide. 1st ed. Cambridge University Press, New York, 2009.

[35] Tahernejad MM, R Khalo Kakaei, M Ataei. Analyzing the effect of ore grade uncertainty in open pit mine planning; A case study of Rezvan iron mine, Iran. Int J Min Geo-Eng. 52 (2018) 53-60, doi: http://dx.doi.org/10.22059/ijmge.2017.234569594678.

[36] Hajizadeh Y, M Christie, V Demyanov. Ant colony optimization for history matching and uncertainty quantification of reservoir models. J Petrol Sci Eng. 77 (2011) 78-92, doi: http://dx.doi.org/10.1016/j.petrol.2011.02.005.

[37] Kotsuki S, CH Bishop. Implementing Hybrid Background Error Covariance into the LETKF with Attenuation-Based Localization: Experiments with a Simplified AGCM. Mon Weather Rev. 150 (2022) 283-302, doi: https://doi.org/10.1175/MWR-D-21-0174.1.

[38] Wernitz S, E Chatzi, B Hofmeister, M Wolniak, W Shen, R Rolfes. On noise covariance estimation for Kalman filter-based damage localization. Mech Syst Sig Process. 170 (2022) 108808, doi: https://doi.org/10.1016/j.ymssp.2022.108808.

[39] Xing X, B Liu, W Zhang, J Wu, X Cao, Q Huang. An Investigation of Adaptive Radius for the Covariance Localization in Ensemble Data Assimilation. J Mar Sci Eng. 9 (2021) 1156, doi: https://doi.org/10.3390/jmse9111156.

[40] Moradi M, O Asghari, G Norouzi, M Riahi, R Sokooti. Joint Bayesian Stochastic Inversion of Well Logs and Seismic Data for Volumetric Uncertainty Analysis. Int J Min Geo-Eng. 49 (2015) 131-42, doi: http://dx.doi.org/10.22059/ijmge.2015.54636.